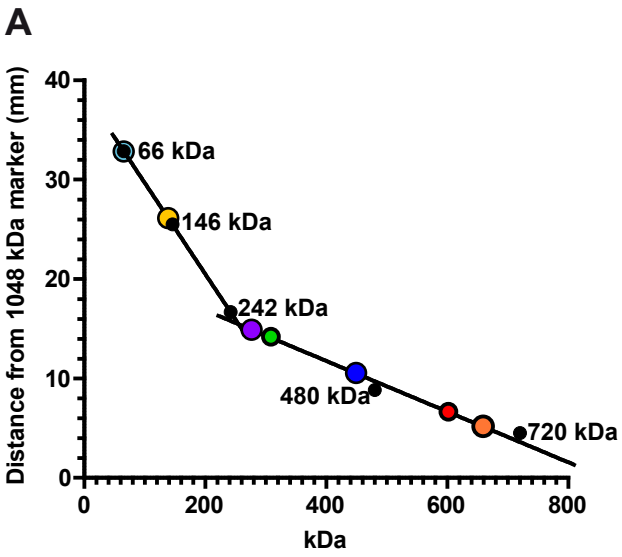

	MW (kDa)	
	Theoretical	*Observed*
Monomers SEPT9_i5-GFP	68	66
Monomers SEPT9_i1-GFP	95	138
Tetramers SEPT9_i1-GFP	236	278
Hexamers	282	308
Octamers SEPT9_i5-GFP	420	450
Octamers	412	602
Octamers SEPT9_i1-GFP	472	660

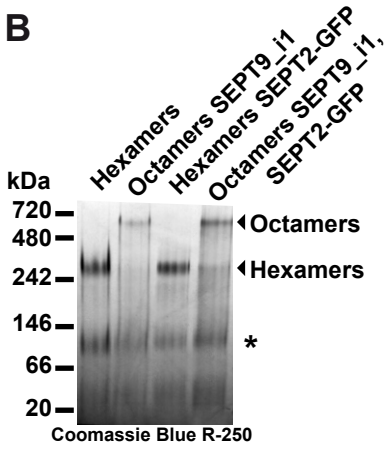

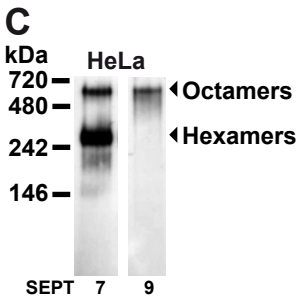

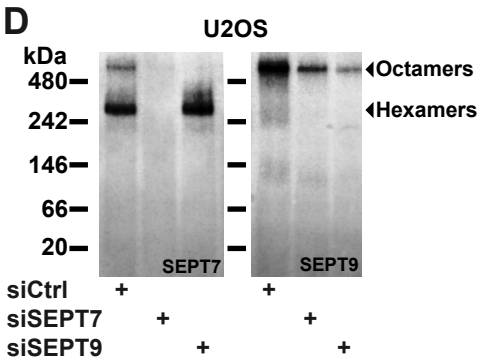

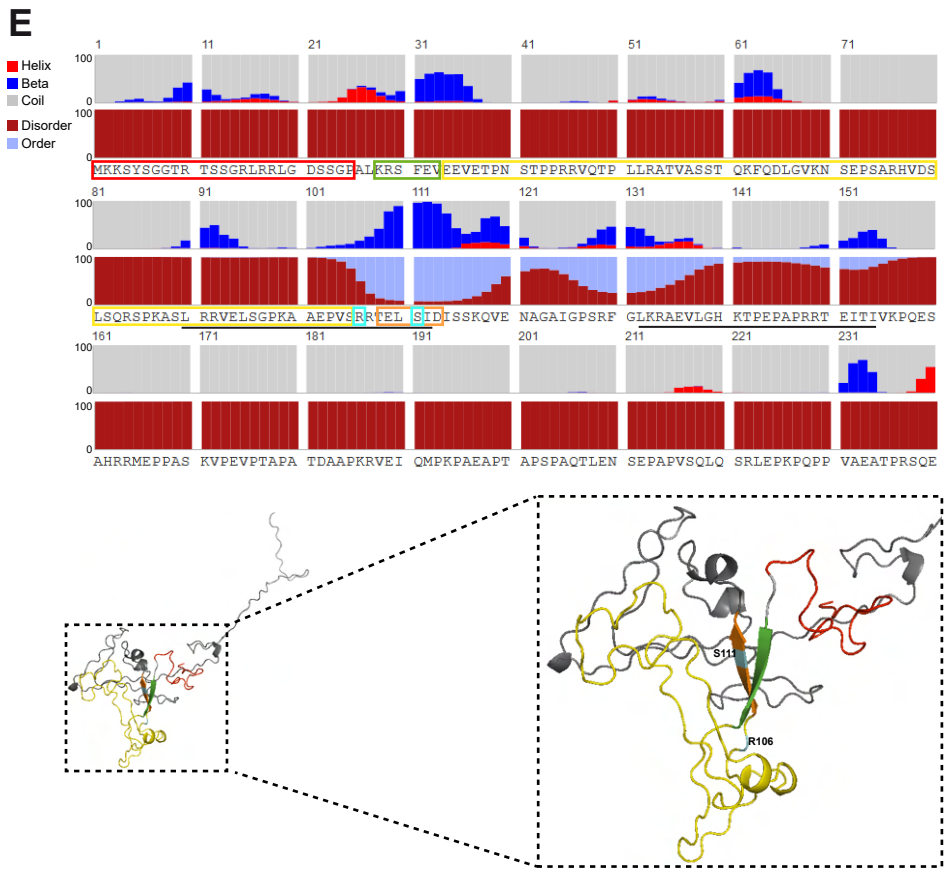

Fig. S1. Separation of septin complexes on native blue gels and detection by Western blot, and structure prediction of SEPT9_i1 region 1-251. (A) Relation between migration distance of native septin complexes from the top of the 4-16% acrylamide gradient gels and migration of MW markers; each data point represents the average of two or three independent determinations. Right: table presenting observed apparent MW and theoretical MW of the different complexes. (B) Recombinant septin hexamers and octamers were run on gradient native gels and were detected by Coomassie blue staining; the asterisk indicates the migration position of putative septin monomers. (C) Native protein extracts from Hela cells were run on native gels and blotted on a PVDF membrane; septin hexamers and octamers were detected by WB. (D) U2OS cells were knocked down for SEPT7 or SEPT9 and native extracts were analyzed as in (C). (E) Top, prediction of secondary structures and disorder in SEPT9_i1 sequence only 1-240 is shown using RaptorX Property Prediction server. Imperfect repeats are underlined with a black line. Bottom, 3D model#2 of the same sequence using RaptorX Contact Predict server. The same color code is used for framed sequences and corresponding portions of the 3D model: red, MBD domain; green, a β-sheet just downstream of MBD; yellow, sequence between the first β-sheet in green and the R106 residue; orange, second β-sheet just downstream of R106; cyan, R106 and S111 residues that are mutated to W and F in HNA patients, respectively.

A

B

Consensus sequence

Fig. S2. Protein sequence conservation of the SEPT9_i1 MBD. (A) Alignment of SEPT9_i1 sequences grouped by phylogenetic proximity: birds and reptiles are highlighted in green and mammals in shades of blue (quadrupeds in dark blue, rodents in purple, and primates in turquoise). Amino acid residues are highlighted based on Clustal X color-coding. A conservation score histogram for each position is presented below the alignments of sequences; under each column is indicated the numerical index reflecting the conservation of physico-chemical properties of amino acid residues (asterisk : 100% identical residues, plus sign: alternative residues with conserved properties). Columns exhibit a color shading coding from the maximal conservation index (11=asterisk) in pure yellow to the minimal conservation index (2) in dark brown. SEPT9_i1 1-25 sequences were recovered using the PSI-BLAST tool and the human sequence as the seed, imported in Jalview, aligned with Mafft (redundant and truncated sequences were eliminated), and grouped by phylogenic proximity by BLOSUM52; the two highly conserved arginine residues R10 and R15 mutated in this study are indicated at the top of alignments. (B) Consensus logo of the SEPT9_i1 MBD was generated using Jalview.

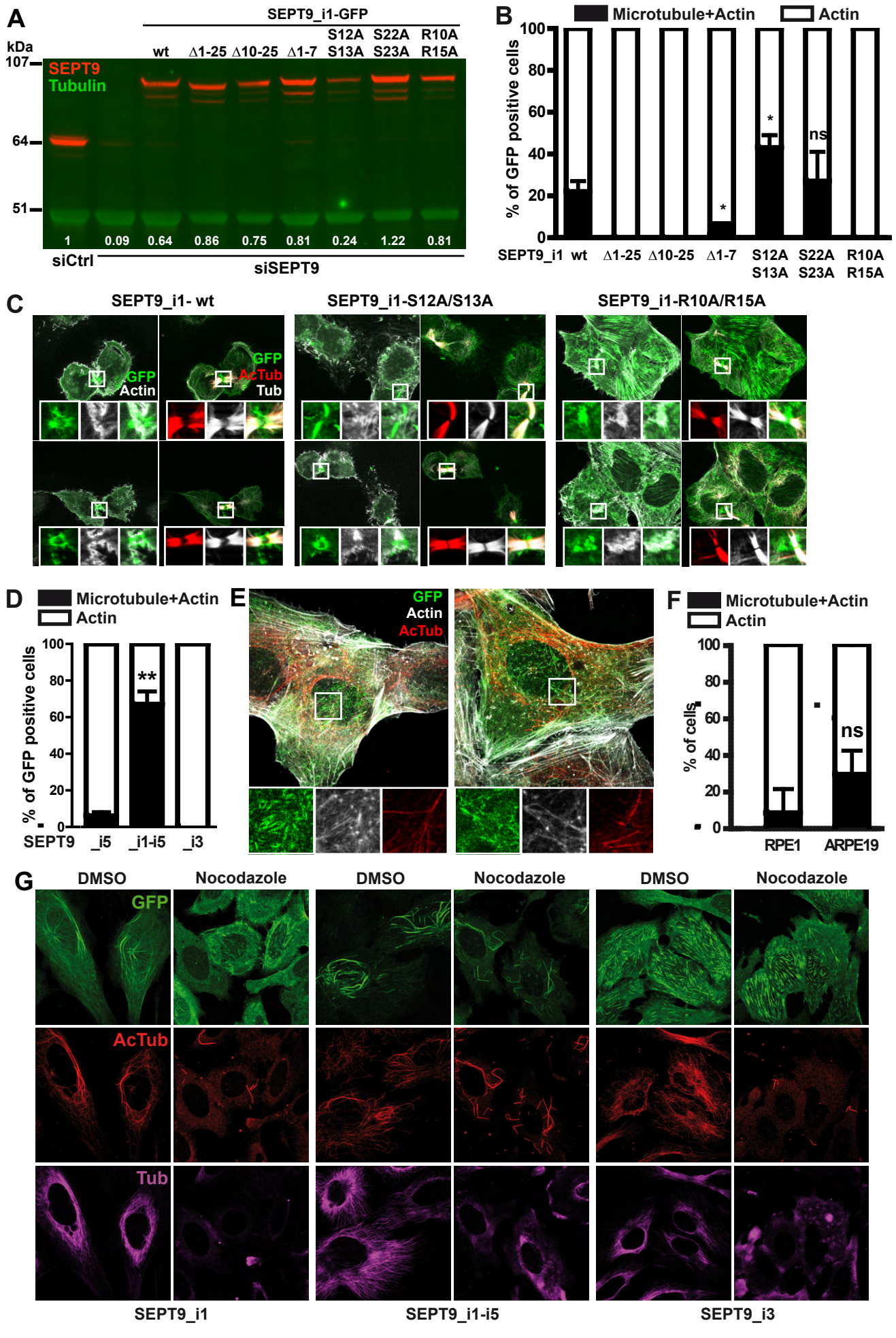

Fig. S3. Cellular localization of SEPT9 by immunocytochemistry. (A) Fluorescent detection of SEPT9 and tubulin on a Western blot of total protein extracts from U2OS cells transiently transfected by a control siRNA (siCtrl) or co-transfected with an siRNA against the 3'UTR region of SEPT9 mRNA (siSEPT9) and with the indicated constructs (described in Fig. 2B). Numbers at the bottom of each lane indicate the levels of expression of SEPT9 constructs relative to those of endogenously expressed SEPT9 (first lane), quantified on this WB. (B) Percentage of U2OS cells, expressing the indicated SEPT9-GFP constructs, displaying co-localization of SEPT9 with microtubules + actin fibers (black) or only actin fibers (white) during cytokinesis, was determined from three independent experiments based on a total of 90 cells (30 cells per experiment). Unpaired, two-tailed t-test with Welch's correction, * $p<0.05$, ns: not significant, microtubule + actin localization relative to SEPT9_i1 wt. (C) Representative images of cells in cytokinesis. Insets are two-fold zoomed regions framed by a white square in the corresponding original images. (D) Percentage of U2OS cells transfected with the indicated SEPT9-GFP constructs displaying co-localization of SEPT9 with microtubules and actin fibers or only actin fibers during cytokinesis was determined from three independent experiments based on a total of 90 cells (30 cells per experiment). Unpaired, two-tailed t-test with Welch's correction, ** $p< 0.01$, microtubule + actin localization relative to SEPT9_i5. (E) Representative images of U2OS cells expressing SEPT9_i5-GFP. Insets are 2.5-fold zoomed regions framed by a white square in the corresponding original images. (F) The percentage of cells displaying co-localization of SEPT9 with microtubules + actin fibers or only actin fibers during cytokinesis in RPE1 and ARPE19 cell lines was determined from three independent experiments based on a total of 90 cells (30 cells per experiment). Unpaired, two-tailed t-test with Welch's correction. (G) Representative images of U2OS cells transfected with the indicated SEPT9-GFP constructs and treated by either vehicle (DMSO) or 10 µM nocodazole for two hours.

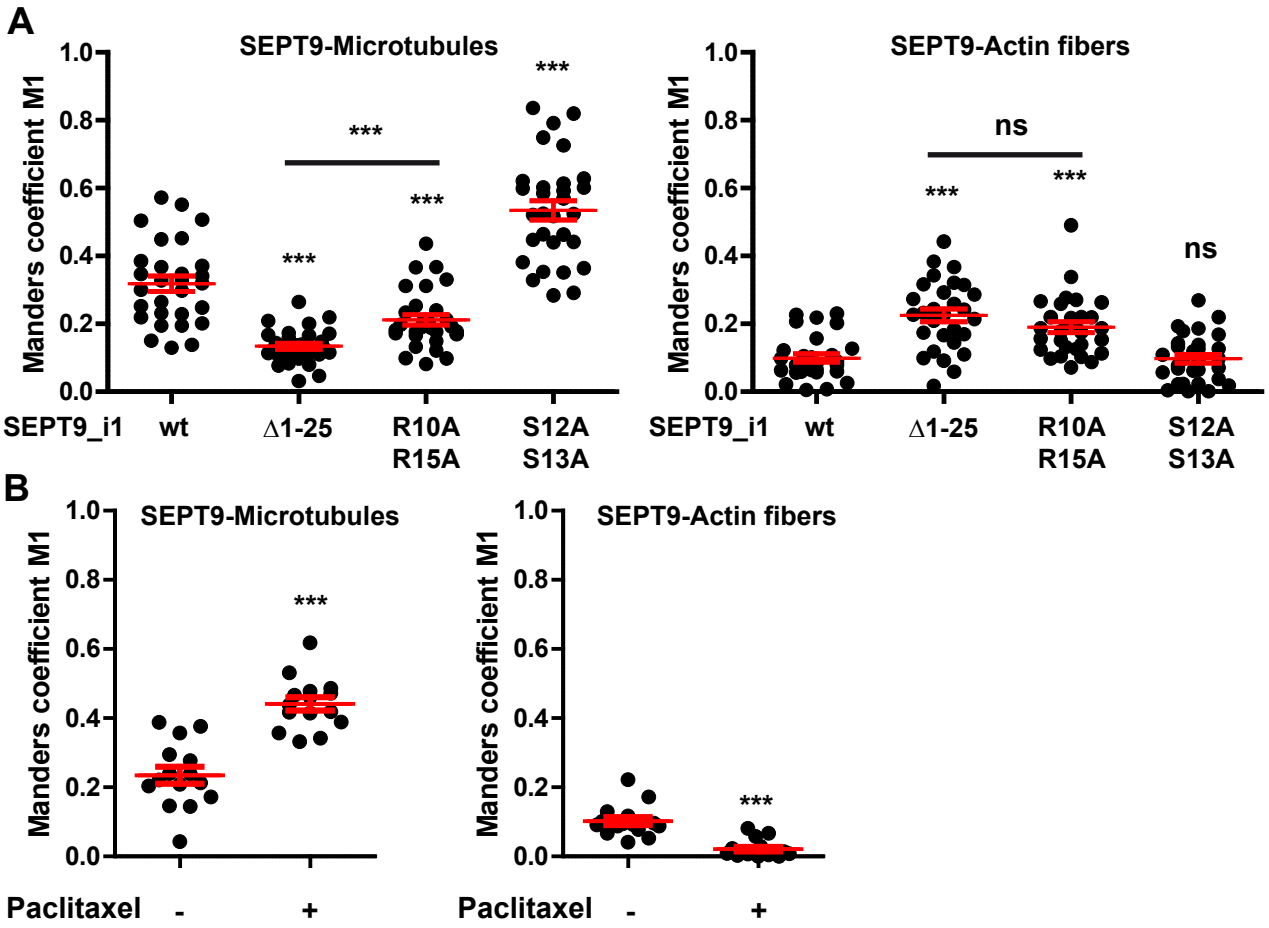

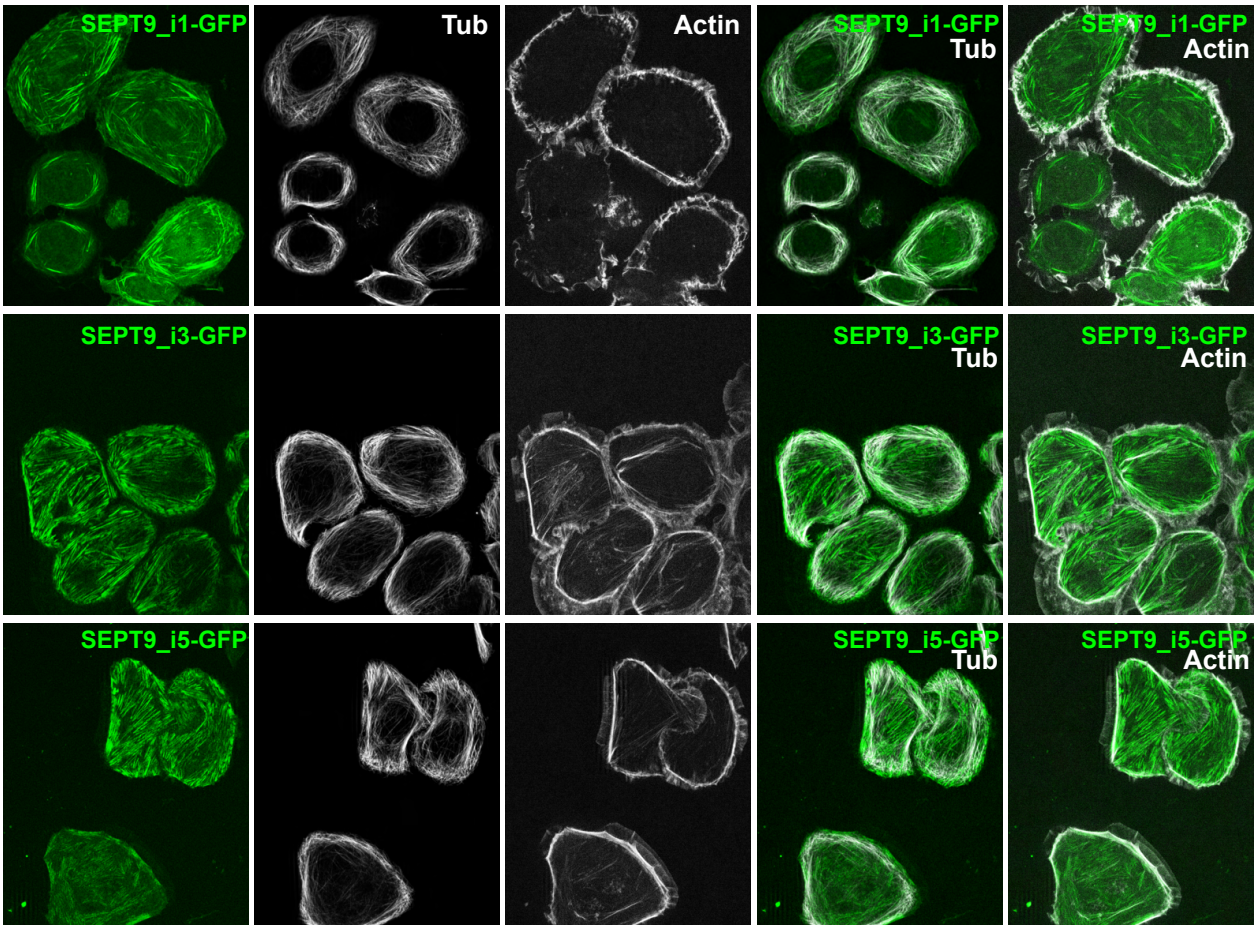

Fig. S4. Quantitation of the extent of SEPT9_i1 wt and mutant co-localization with microtubules or actin fibers within individual cells. (A) Manders M1 coefficients for co-localization of indicated SEPT9-GFP constructs expressed in SEPT9 knockdown U2OS cells with microtubules or actin fibers. Analysis was performed in 30 individual cells for each condition. (B) Manders M1 coefficient for co-localization of SEPT9_i1-GFP construct transfected in SEPT9 knockdown SKBr3 cells with microtubules or actin fibers. Seventy hours after transfection, cells were treated with either 0.002% DMSO or 2 μM paclitaxel for two hours. Analysis was performed in 15 individual cells for each condition. Unpaired, two-tailed t-test with Welch's correction, *** $p<0.0001$, ns: not significant. (C) Microtubule immunofluorescence, fluorescent phalloidin, and GFP fluorescence images of SEPT9 knockdown SKBr3 cells transfected with SEPT9_i1, _i3 or _i5-GFP constructs and treated with paclitaxel as in (B). Scale bar 10 μm.

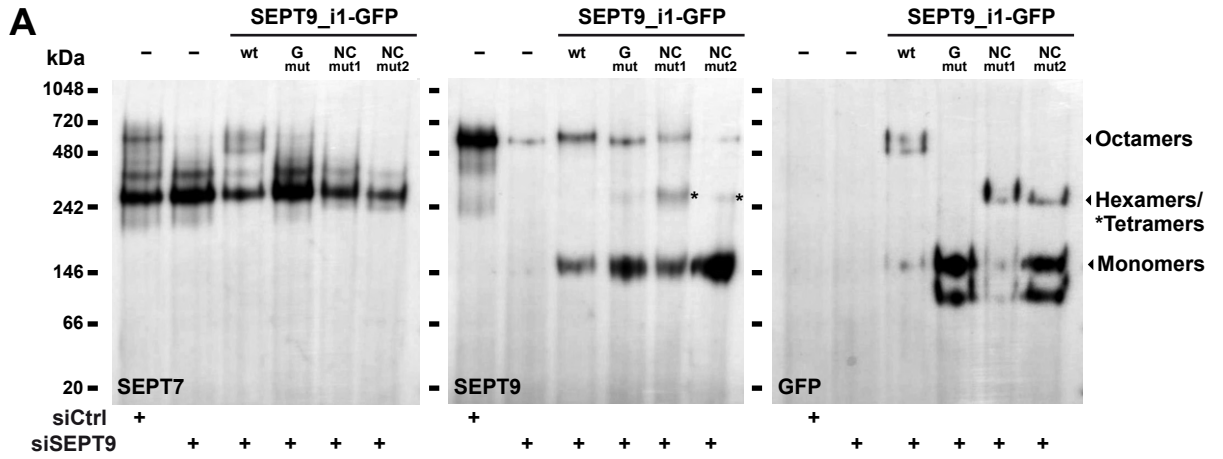

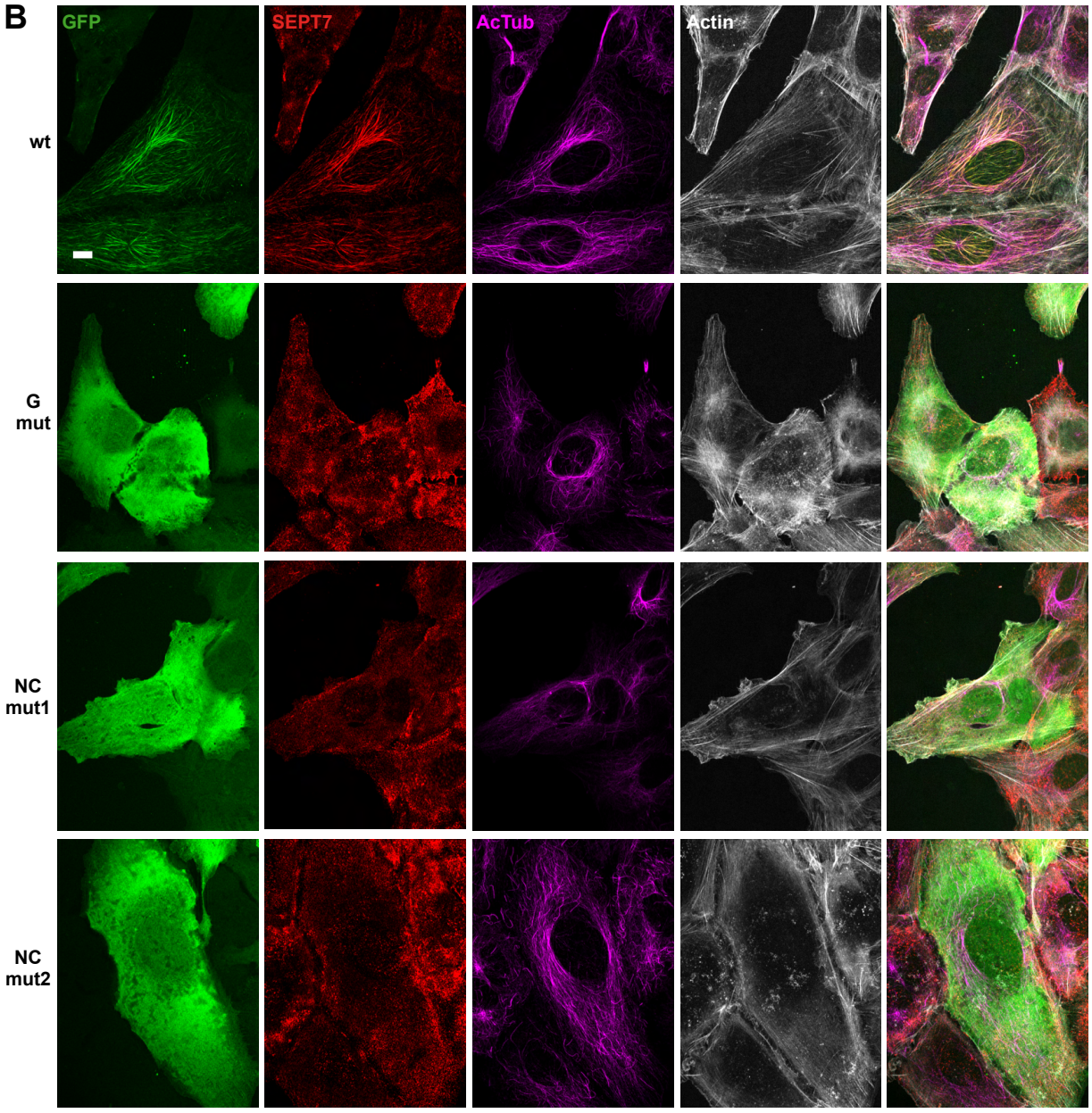

Fig. S5. Effects of SEPT9_i1 G or NC interface mutants on septin complex assembly and localization. (A) Western blots of native gels resolving septin complexes present in U2OS cells transfected with indicated siRNA and expressing SEPT9_i1 wt or SEPT9_i1 interface mutants. (B) Representative images of GFP-fluorescence based co-localization of SEPT9_i1 wt or interface mutants with SEPT7, actin and acetylated microtubules; SEPT9_i1 wt co-localized both with microtubule and actin fibers as expected, but non-octameric septin complexes containing an SEPT9_i1 interface mutant did not. SEPT7 co-localized with SEPT9_i1 wt, but localized in patches independent of the diffuse localization of SEPT9_i1 interface mutants. Scale bar 10 µm.

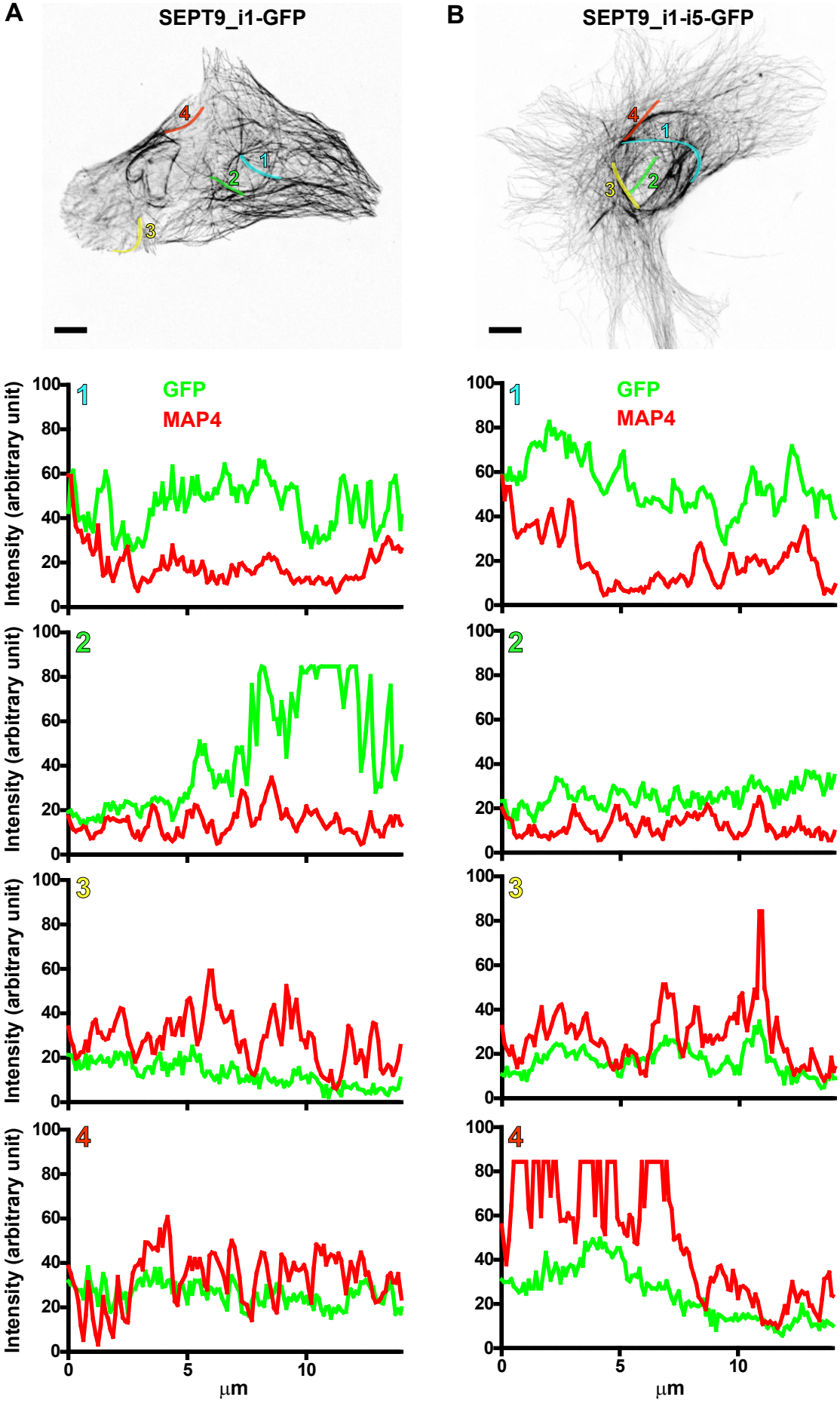

Fig. S6. MAP4 poorly localizes to microtubule bundles where SEPT9_i1 wt or SEPT9_i1-i5 accumulates. Four examples of fluorescence profiles associated with microtubule bundles (each bundle is highlighted and numbered in corresponding color in images) for MAP4 (immunofluorescence) and GFP (SEPT9 constructs) in cells expressing either SEPT9_i1 wt (A) or SEPT9_i1-i5 (B) are presented under the images of cells from Fig. 4B. Bundles with SEPT9_i1 or SEPT9_i1-i5 accumulation were more frequently seen towards the center of cells, near the nucleus (bundles numbered 1 and 2). Of note, in order to outline microtubule bundles, images correspond to grey scale negatives of merged images of microtubules and acetylated microtubules subpopulation (the latter is not presented in Fig. 4B).

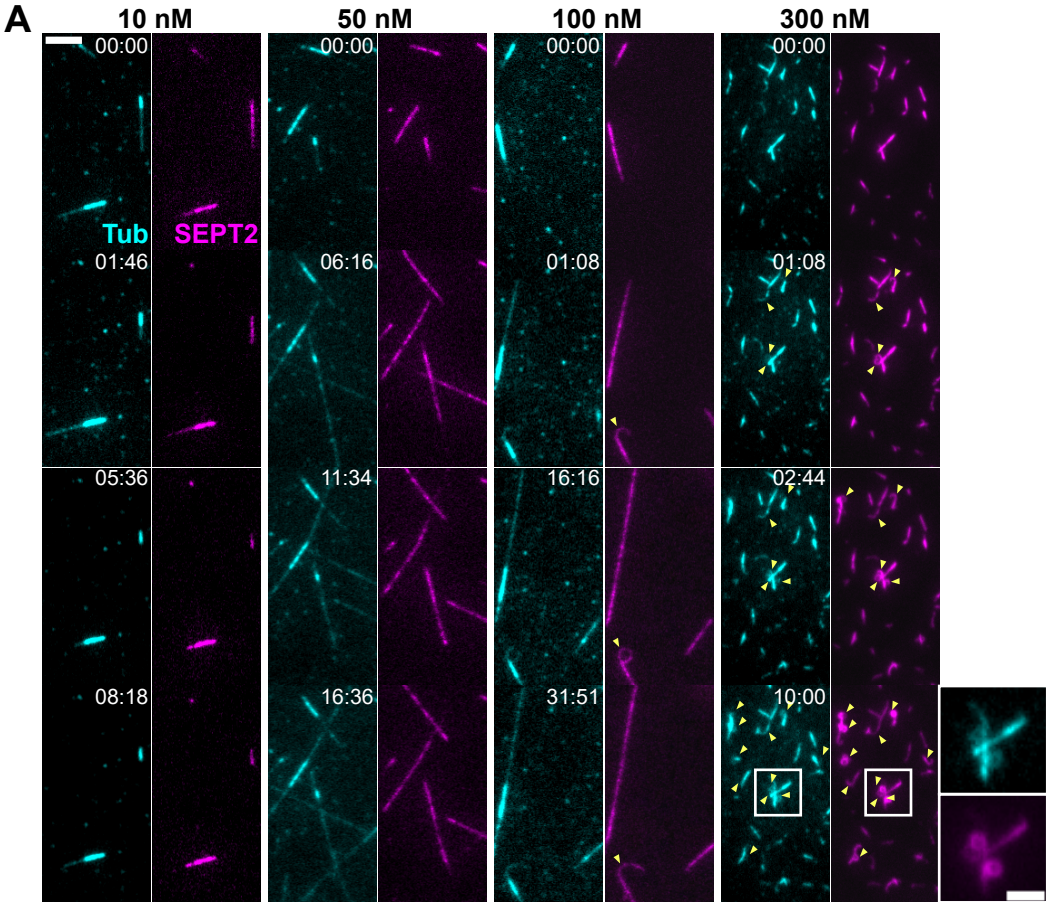

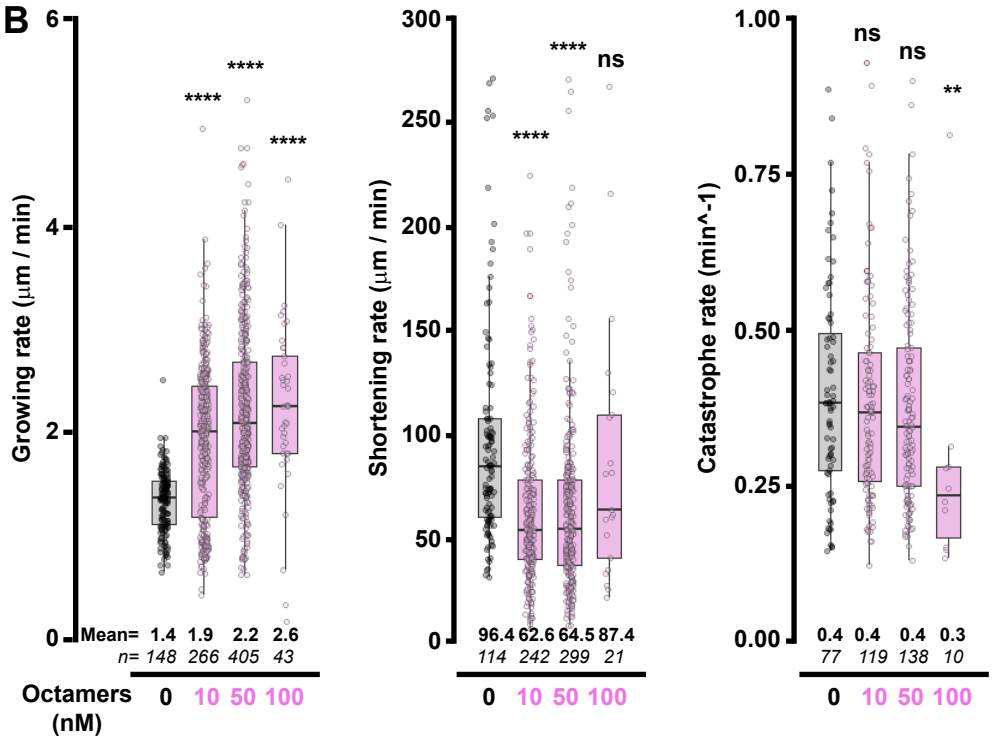

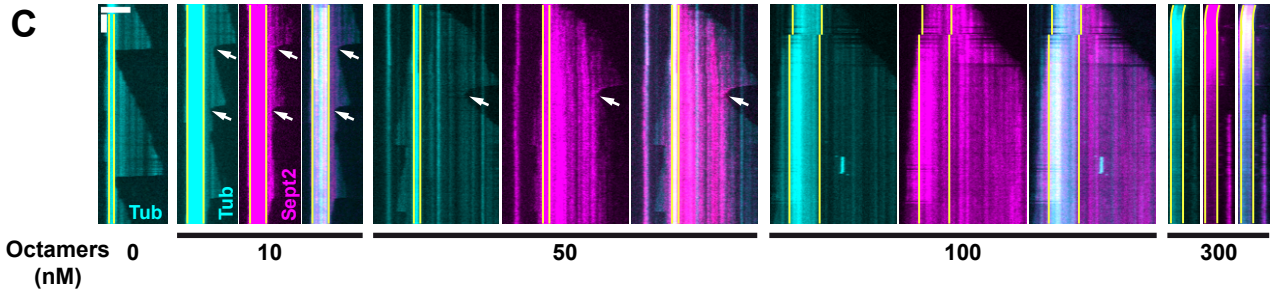

Fig. S7. Binding of octamers harboring SEPT9_i1-i5 (Oct9_i1-i5) on microtubules and their effect on microtubule dynamics. (A) Still images from time lapse TIRF movies of Oct9_i1-i5 interacting with dynamic microtubules at different concentrations in the range of 10-300 nM. Time indicated on each set of images is in min:sec. Yellow arrowheads indicate curved and loop-like structures present at the plus-ends of growing microtubules. The inset shows a close-up of these loops after 10 min with 300 nM Oct9_i1-i5. Scale bar 5 μm in the main images and 2μm in zoomed framed region. (B) Quantitation of microtubule dynamic parameters (growth, shortening and catastrophe rates) at increasing septin octamer concentrations. Results from two independent experiments are presented as whisker boxes (median value horizontal bar in each box with 5-95 percentile range) superposed with individual data points. The result of a two-tailed t-test with Benjamini & Hochberg p-value correction with R comparing each sample with the control (no octamers) is shown above each whisker box (* $p<0.05$, ** $p<0.01$, *** $p<0.001$, **** $p<0.0001$, ns: not significant). (C), Representative kymographs. Horizontal scale bar 5 μm; vertical scale bar 50 sec. White arrows indicate rescues. Vertical yellow lines indicate the borders of the GMPCPP-stabilized microtubule seed.

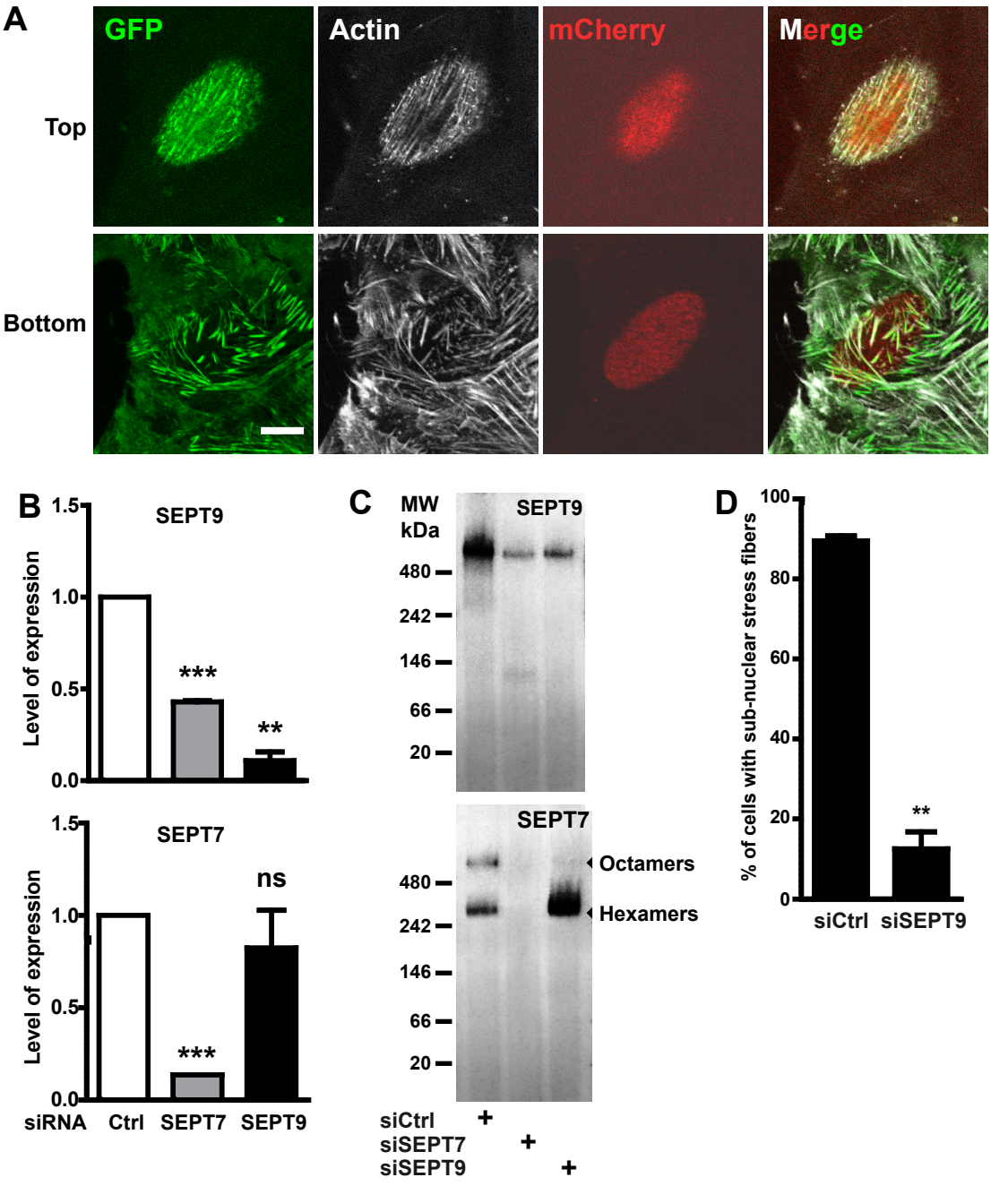

Fig. S8. Phenotyping of cells based on the presence of sub-nuclear actin fibers, and characterization of U2OS cell lines stably co-expressing SEPT9-GFP and mCherry-H2B constructs. (A) Top and bottom view of actin fibers (phalloidin-Atto 390), SEPT9_i1 (GFP), and nucleus (mCherry-H2B) in a U2OS.SEPT9_i1-GFP cell. Scale bar 10 µm. (B) Effects of SEPT7 or SEPT9 knockdown in RPE1 cells on the relative expression of SEPT7 and SEPT9 analyzed by WB and (C) on the presence of hexamers and octamers, analyzed by Western blots of native extracts resolved on native 4-16% acrylamide native gels. In (B), Western blot signals of SEPT7 or SEPT9 expression were first normalized to the respective Western blot signals of α-tubulin and further normalized to the ratio obtained from cells transfected with Ctrl siRNA; results are from three independent experiments. Paired, two-tailed t-test with Welch's correction, ** $p< 0.01$, *** $p<0.0005$, ns: not significant. (D) Quantification of the presence of sub-nuclear actin fibers in SEPT9 knockdown RPE1 cells KD in the absence of octamers. Results are from three independent experiments for a total of 90 cells (30 cells per experiment). Unpaired, two-tailed t-test with Welch's correction, ** $p< 0.01$. (E) Expression of SEPT9-GFP constructs (SEPT9_X-GFP) and total endogenous SEPT9 (top Western blot) and expression of SEPT9_i3-GFP constructs and endogenous SEPT9_i3 (bottom Western blot) in U2OS cell lines stably co-expressing mCherry-H2B and SEPT9-GFP constructs (U2OS.SEPT9_X-GFP) and in the non-transfected parental U2OS cell line. (F) Percentages of cells displaying co-localization of SEPT9_X-GFP with microtubules and actin fibers in U2OS.SEPT9_X-GFP cell lines. Results are from one determination in 30 cells from each cell line.

Table S1. Microtubule dynamic parameters for conditions depicted in Fig. 6, 7.

Click here to download Table S1

Table S2. Microtubule dynamic parameters for conditions depicted in Fig. S7.

Click here to download Table S2

Table S3. Oligonucleotide primer sequences used for the generation of the plasmids used in this study. Oligonucleotides marked with an asterisk are shared among several constructs, but are listed only once.

Click here to download Table S3

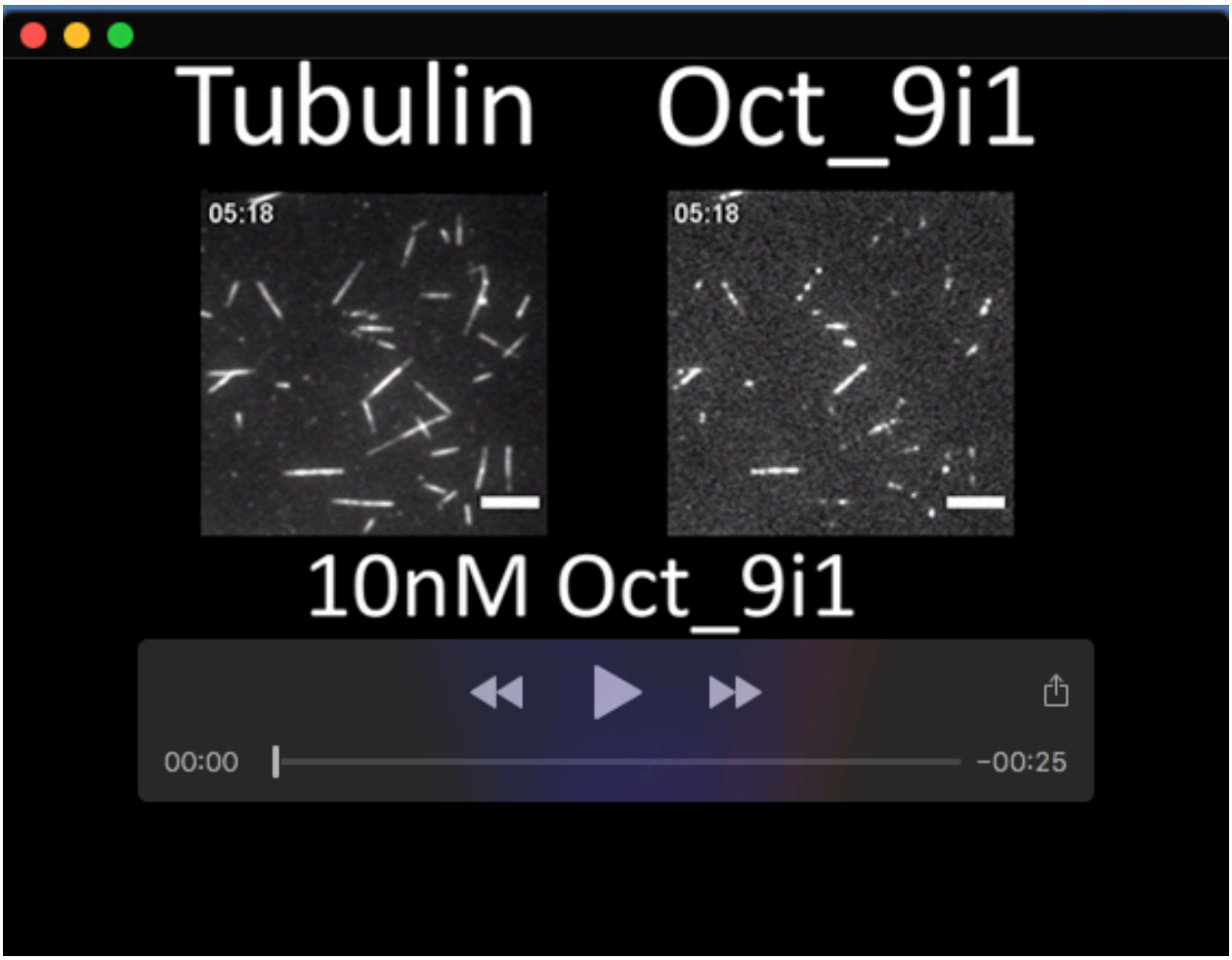

Movie 1. Dynamics of septin octamers harboring SEPT9_i1 (Oct_9i1) binding with microtubules *in vitro*. Series of videos corresponding to each of the 10 to 300 nM concentrations of Oct_9i1 that were used. Scale bar 5 µm.

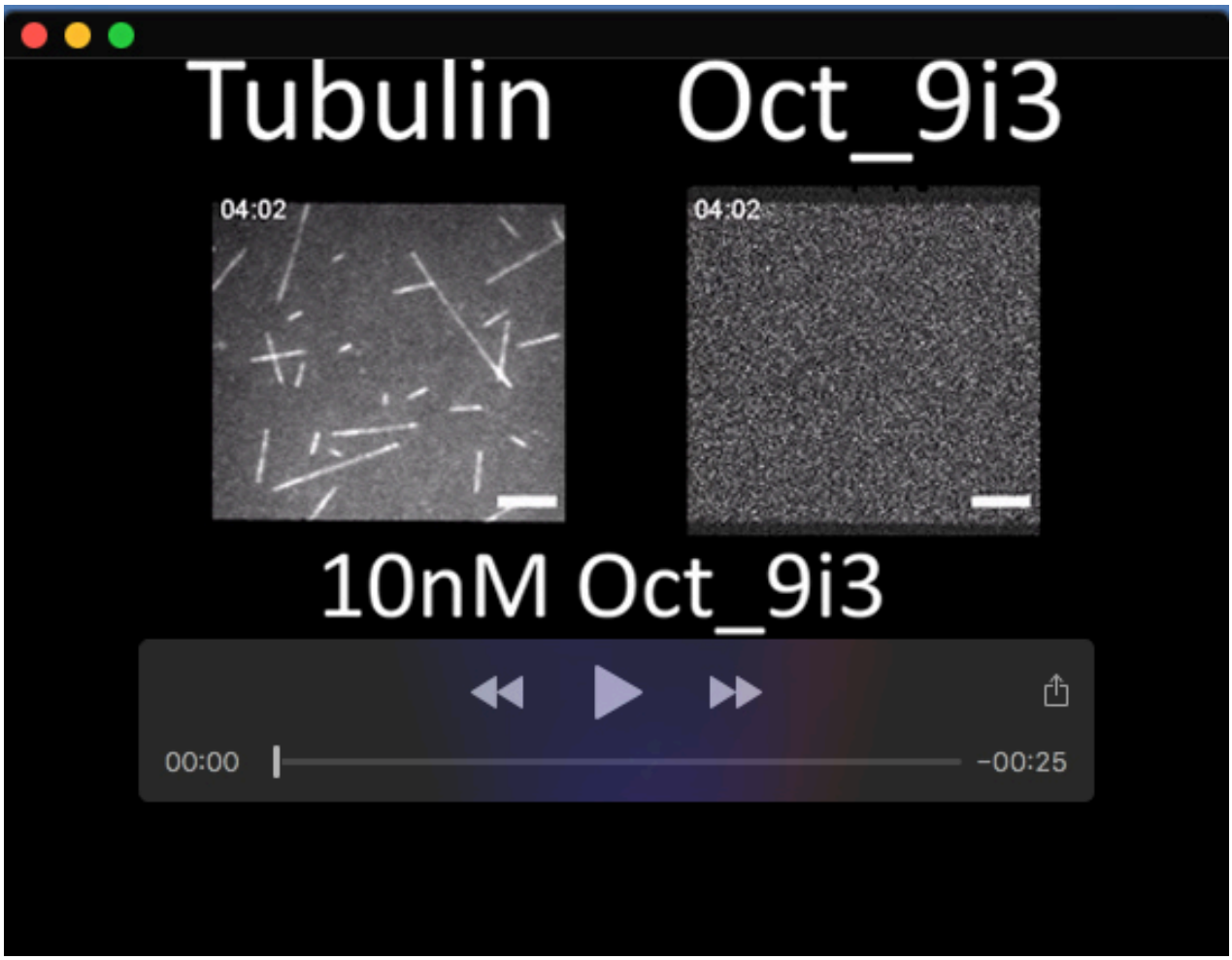

Movie 2. Dynamics of septin octamers harboring SEPT9_i3 (Oct_9i3) binding with microtubules *in vitro*. Series of videos corresponding to each of the 10 to 300 nM concentrations of Oct_9i3 that were used. Scale bar 5 µm.

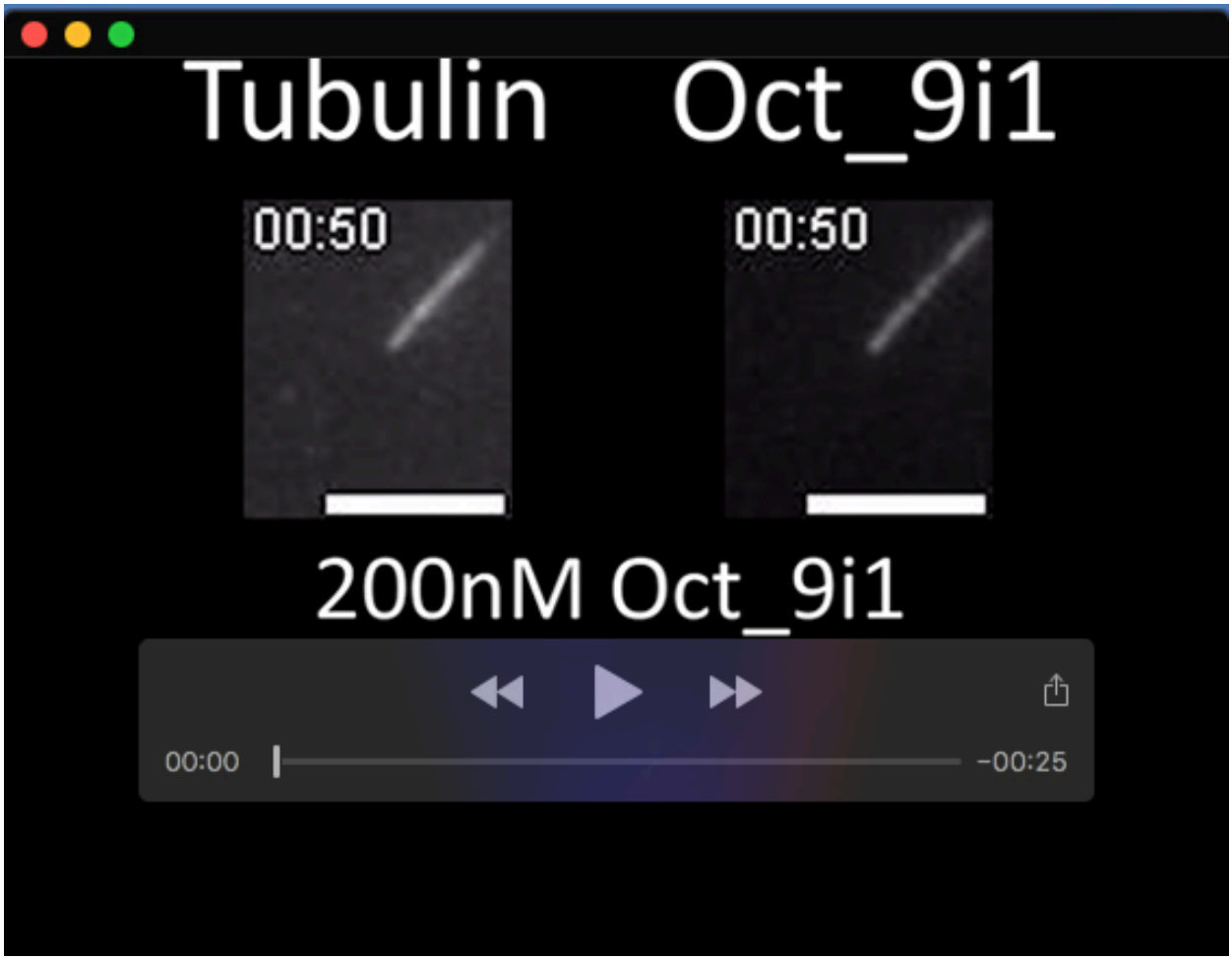

Movie 3. Depolymerizing microtubules in presence of 200 nM of septin octamers harboring SEPT9_i1 (Oct_9i1) *in vitro*. Series of videos corresponding to examples 1 and 2. Scale bar 5 µm.

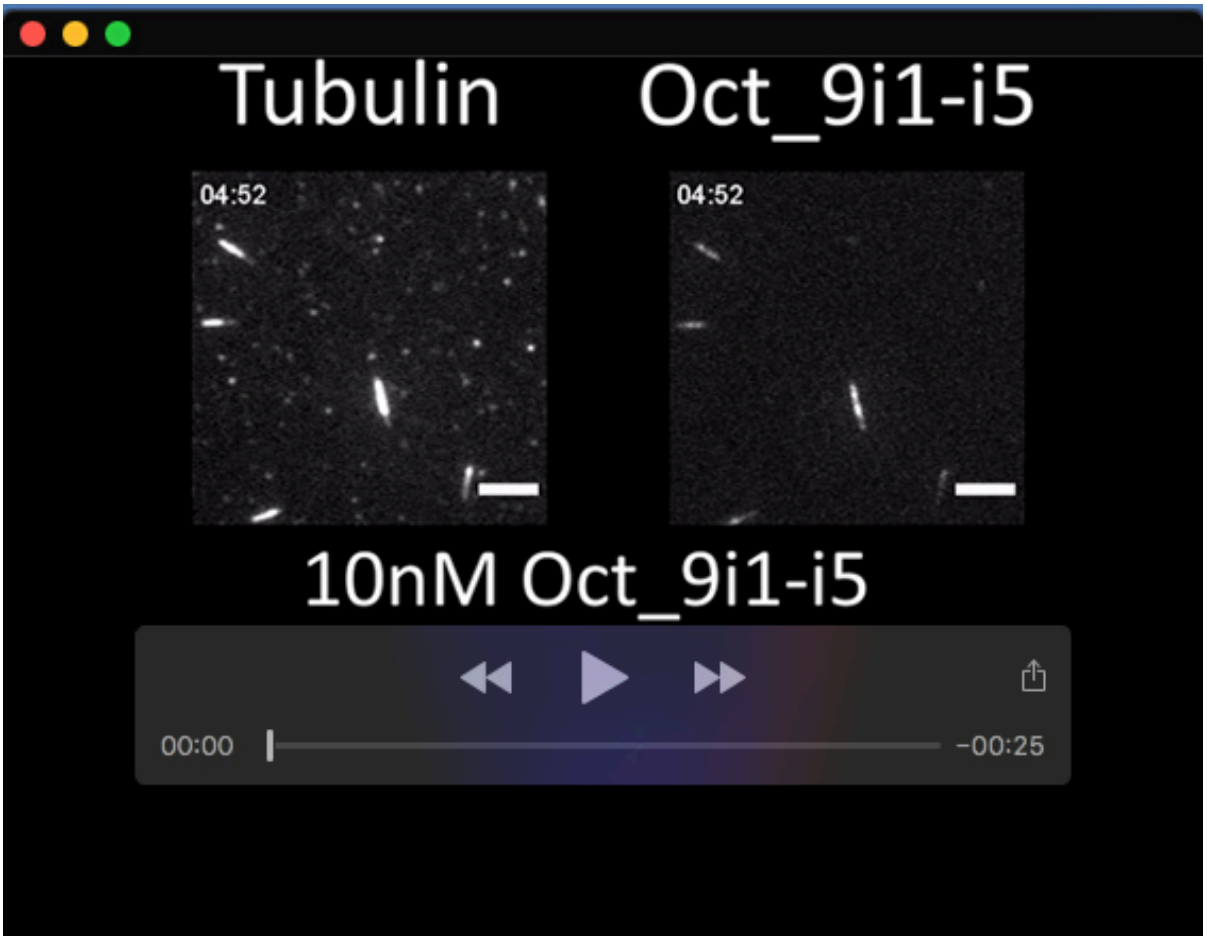

Movie 4. Dynamics of septin octamers harboring SEPT9_i1-i5 (Oct9_i1-i5) binding with microtubules *in vitro*. Series of videos corresponding to each of the 10 to 300 nM of Oct_9i1-i5 that were used. Scale bar 5 µm.